Journal of
Marine Science and Engineering

Article

Spot Charter Rate Forecast for Liquefied Natural Gas Carriers

Dimitrios V. Lyridis

Laboratory for Maritime Transport, School of Naval Architecture and Marine Engineering, National Technical University of Athens, 15773 Athens, Greece; dsvlr@mail.ntua.gr

Abstract: Recent maritime legislation demands the transformation of the transportation sector to greener and more energy efficient. Liquified natural gas (LNG) seems a promising alternative fuel solution that could replace the conventional fuel sources. Various studies have focused on the prediction of the LNG price; however, no previous work has been carried out on the forecast of the spot charter rate of LNG carrier ships, an important factor for the maritime industries and companies when it comes to decision-making. Therefore, this study is focused on the development of a machine learning pipeline to address the aforementioned problem by: (i) forming a dataset with variables relevant to LNG; (ii) identifying the variables that impact the freight price of LNG carrier; (iii) developing and evaluating regression models for short and mid-term forecast. The results showed that the general regression neural network presented a stable overall performance for forecasting periods of 2, 4 and 6 months ahead.

Keywords: machine learning; forecast; regression models; liquified natural gas; maritime transportation

check for updates

Citation: Lyridis, D.V. Spot Charter Rate Forecast for Liquefied Natural Gas Carriers. *J. Mar. Sci. Eng.* **2022**, *10*, 1270. https://doi.org/10.3390/jmse10091270

Academic Editor: Claudio Ferrari

Received: 22 July 2022
Accepted: 22 August 2022
Published: 8 September 2022

1. Introduction

Maritime fuel combustion is estimated to contribute 3% of the annual global greenhouse gas emissions [1]. The International Maritime Organization (IMO) regulations on marine fuel impose the need for greener transportation. These regulations include the limitation to sulfur emissions in certain control areas (SECAs) and nitrogen oxide emission control areas (NECAs), while they encourage alternative fuel sources that will contribute to the increase in greenhouse gas emissions and capital investments [2]. A promising alternative solution for fuel is liquefied natural gas (LNG) [3,4]. In 2020, the International Gas Union (IGU) reported a significant increase in the number of terminals for LNG liquefaction and regasification. Moreover, the European Commission, in the context of Clean Power for Transport Directive, has supported the deployment of alternative fuels as well as recharging and refueling infrastructure. Furthermore, the evidence shows the gradual development of short-term and spot LNG markets and consequently the corresponding shipping market [5]. The annual report of 2020 for the LNG industry from GIIGNL showed the increase in share of spot and short-term LNG market compared to the total LNG trade [6]. Following the unconventional gas revolution, the forecasting of natural gas prices and moreover the freight prices of LNG bunkering ships have become important due to the low correlation of these prices with those of crude oil [7].

Machine learning and artificial intelligence analytics have been commonly employed for forecasting prices of fuels [8,9] in the energy and marine sectors. Recent studies have highlighted the necessity of adopting alternative fuels for more sustainable marine transportation, proposing liquefied natural gas (LNG) as a greener ship fuel [10,11]. To this end, the scientific community has turned its attention to the study of LNG as ship fuel in the marine sector, focusing on economic feasibility, safety analysis, and decision-making models regarding the use of LNG [11–14].

Various studies have been conducted regarding the forecasting of price of LNG. Specifically, in [15], hybrid models based on the combination of wavelets, time series and artificial neural networks (ANNs) have been proposed in order to predict the price of natural gas. An autoregressive neural network (ARNN) model was presented in [16] for predicting natural gas spot prices. A least squares regression boosting (LSBoost) algorithm was applied for data-driven daily, weekly, and monthly forecasts of natural gas spot price on Henry Hub time series [17]. In the context of the implementation of this work, an analysis of potential influence factors regarding the spot price movements of natural gas was conducted based on a nonlinear autoregressive neural network with exogenous inputs (NARX) [18]. However, the study was limited to the market area NetConnect Germany (NCG). Time series and various artificial neural network (ANN) models were also adopted in another study [19] aiming at predicting the price of natural gas in the United States market. Another study for a specific market was conducted at a regional scale in Turkey [20], where an artificial bee-colony-based artificial neural network (ANN-ABC) was developed to forecast the day-ahead demand of natural gas. From company perspective, a stochastic programming approach was adopted for an optimal planning of LNG purchase for oil and gas companies [21]. Hence, the model aimed at predicting the demand and the prices of LNG in a planning horizon.

In [22], a combination of two nonparametric methods, namely rescaled range analysis and multifractal detrended fluctuation analysis, was presented for statistical analysis with respect to the correlation, fluctuation, and scaling of the freight process in the liquid petroleum gas shipping market. Another statistical analysis was performed in [23]. The aim of this study was to identify the multiple financial and shipping-related measures that have a statistically significant contribution to the prediction of the spot voyage time charter price of the P1A Panamax shipping route. In [24], linear and nonlinear methods were evaluated for short-term forecasts in the dirty tanker shipping market. Serial time series and neural networks were involved in this study for a more accurate prediction of freights that will support the decision-making of maritime companies. An extension of [24] is presented for freight rate derivatives to improve the prediction accuracy of the models [25]. ANNs were also employed for modeling the Baltic dry bulk shipping market trained by macroeconomic factors and shipping market parameters [26]. Specifically, an ANN was trained by using real data for a 20-year period for a wide range of macroeconomic factors (19) and maritime indexes (four). A similar study focusing on the dry bulk shipping market on the BPI T/C and BCI C7 routes was conducted in [27], where the vector autoregression and the vector error connection models were applied to identify the dynamics and interactions between spot and forward freight agreement prices. In [28], an adynamic probit model was developed to forecast the future weekly, quarterly, and biyearly changes of spot freight rates for Panamax dry bulk ships [28]. To forecast the value-at-risk (*VaR*) of dry bulk shipping markets, nine different risk models were developed and evaluated in [29]. Regarding the crude oil market, the periodic variation law of the tanker market was studied based on quantitative methods. The work investigates the cycle duration and amplitude of different scales of an Aframax tanker's freight to predict the long-term variation trend of freight rate on that basis.

While various studies have been conducted on the forecast of LNG price and the charter rates in various shipping markets, to the best of our knowledge, no previous work has been implemented regarding the forecast of the charter rates in the LNG shipping market. This is especially important as any increase in LNG demand as marine fuel will be interconnected with increased demand of LNG transportation service via LNG carriers, from liquefaction terminals to local storage and bunkering hubs. To this end, this study contributes to the development of a machine learning approach for:

Identifying the features that contribute to the accurate prediction;

Employing various neural networks for forecasting the charter rate of LNG carriers for 2, 4 and 6 months in the future;

Evaluation of the predictive models and comparisons with respect to the forecasting of LNG 145K CDM spot rate on 1 March 2017, 1 May 2017 and 1 July 2017 based on time series data from 1 January 2010 to 1 January 2017.

This paper is organized as follows. Section 2 gives a description of the dataset that was used in our study. In Section 3, the proposed methodology along with the necessary feature selection and validation mechanisms are presented. Results are given in Section 4. Conclusions and future work are outlined in Section 5.

2. Materials and Methods

2.1. LNG Data

The data relevant to LNG were collected from multiple data sources where access was available (Table 1). In the first column of Table 1, the data sources are shown from where time series data relevant to LNG market were collected. These data sources include the Clarkson PLC Shipping Intelligence Network, the GIIGNL International Group of LNG Importers, the U.S. Energy Information Administration (EIA) and the BP Statistical Review of World Energy. These data were chosen due to their impact on LNG market. The data collection was focused on the chronological period from 1 January 2010 to 1 January 2017, since the short-term market was significantly increased from 2010 onwards.

Table 1. Data sources and the time series used in the methodology.

Data Source	Data Description of Time Series
Clarkson PLC Shipping Intelligence Network	LNG 145K CBM spot rate (USD/day): the desired prediction variable. It represents the price of the daily fare for an LNG tanker with a capacity of 145,000 CBM and a steam turbine vessel. LNG 160K CBM spot rate (USD/day): the price of the daily fare for an LNG tanker with a capacity of 160,000 CBM, tri-fuel diesel electric (TFDE). LNG 160K CBM 1 Year Timecharter Rate (USD/day) presents the price of the daily fare for one-year contracts for a ship with the same characteristics as above. World Seaborne LNG Trade (million tonnes) reveals the demand for LNG regarding the quantity that is traded internationally. World Seaborne LNG Trade (billion tonne-miles) represents the trade of LNG, multiplied by the distance that the commodity has traveled. Import LNG Japan Price (USD/mmbtu): the import price of LNG in Japan. Total LNG Fleet reveals the number of vessels that transport LNG. Total Shipping Capacity (m^3—CBM) is related to the offer and shows the total capacity of all LNG vessels. Operational Capacity (m^3—CBM) presents the total operating capacity for trading LNG. Its combination with the operating capacity shows the percentage of ships that are inactive at a specific time in the market. New Orders Placed indicate the attitude of shipowners toward the future of the LNG market. Orderbook shows reflects the capacity and the ability of shipyards to accept new orders in near future. Ships Delivered That Year presents the number of ships that the shipyards deliver in that year.
GIIGNL International Group of LNG Importers	Liquefaction Plants/Liquefaction (million tonnes per annum—MTPA) presents the amount of gas that is liquefied. While new liquefaction plants are being built, it shows that the market is on the rise. Liquefaction Plants/Storage (m^3—CBM) directly affects the short-term purchase of LNG. The storage capacity was one of the main factors that led to the rise of the short-term market, allowing sellers to keep the quantities they produce and dispose of them whenever they consider it necessary. Regasification Plants/Storage (m^3—CBM) shows the evolution of the ability to store LNG in regasification stations. Regasification Plants/Sent Out (billion cubic meters—bcm/year) refers to the annual quantities of LNG that is gasified. Spot LNG Imports (million tonnes) is linked with the quantities of LNG imported under the direct delivery regime.

Table 1. *Cont.*

Data Source	Data Description of Time Series
U.S. Energy Information Administration (EIA)	Price of Liquefied U.S. Natural Gas Exports (USD/thousand cubic feet): the price of LNG exported by the USA. Henry Hub Natural Gas Spot Price (USD/million btu): Henry Hub is a gas pipeline located in Louisiana, USA. It is the pricing reference point for gas contracts traded on the New York Mercantile Exchange (NYMEX). Settlement prices are used as benchmarks for the entire North American gas market as well as for parts of the global LNG market. It is an important indicator as the price of natural gas is based on real supply and demand as a standalone commodity. WTI Oil Price (USD/barrel): West Texas Intermediate (WTI) crude oil is the basis for New York oil futures contracts. This indicator is important as it is a reference point for buyers and sellers of oil. Brent Oil Price (USD/barrel): Brent is a blend of crude oil exported from the North Sea. It is the reference point for most of the crude oil in the Atlantic basin and it is used to price two thirds of the crude oil traded internationally.
BP Statistical Review of World Energy	Worldwide Natural Gas Production (billion cubic meters—bcm) shows the global production of natural gas. Worldwide Natural Gas Consumption (billion cubic meters—bcm) shows the global consumption of natural gas.

2.2. Methodology

To predict the price of a specific product/index in the market, a common approach is to identify the correct data to use, adopt a pre-process methodology to transform them and identify certain patterns for knowledge extraction. These approaches are commonly implemented via machine learning techniques [30,31]. The proposed machine learning pipeline consists of the following steps: (i) the variables selection process and (ii) development and evaluation of prediction models. The selection of features is realized based on the Pearson product-moment correlation coefficient (PCC) whereas various prediction models, such as regression models and neural networks, are applied and compared with respect to the forecast of the price of the daily charter rate for an LNG tanker with a capacity of 145,000 CBM (LNG 145K CBM spot rate).

2.2.1. Variables Selection

The correlation between the prediction variable, LNG 145K CBM spot rate, and the other independent variables, which are described in Table 1, was calculated based on the Pearson product-moment correlation coefficient, $\rho_{X,Y}$, [32,33] for a time horizon of 2, 4 and 6 months. The PCC was used to identify the variables with high linear correlation with respect to the selected decision variable in order to be used for the development of the prediction models.

Let X and Y be two zero-mean real-valued random variables. The PCC is defined as:

$$\rho_{X,Y} = \frac{cov(X,Y)}{\sigma_X \sigma_Y} \tag{1}$$

where $cov(X,Y)$ is the covariance of the two variables X and Y, and σ_X, σ_Y are the standard deviation of X and Y, respectively. The covariance $cov(X,Y)$ is given by:

$$cov(X,Y) = E[(X-\mu_X)(Y-\mu_Y)] \tag{2}$$

where μ_X, μ_Y are the mean of X and Y, respectively. The values of the PCC range $-1 < \rho_{X,Y} < 1$.

2.2.2. Data Regression

Machine learning (ML) has been widely applied to regression estimations in various domains. ML techniques extract prior knowledge by restricting the space of assumed dependencies without making any distributional assumptions [34]. Typical regression approaches include moving average and ARIMA models [35]. Moving average is a classical method. A moving average of order n can be written as:

$$\hat{Y}_t = \frac{1}{n}\sum_{j=-k}^{k} y_{t+j} \tag{3}$$

where $n = 2k + 1$. It expresses the estimation of the trend cycle at time t, obtained by averaging values of the time series within k periods of t.

One of the most powerful ML algorithms is the artificial neural network (ANN) [36]. An ANN consists of a collection of processing elements, such as neurons or nodes, which are fully or partially interconnected. Its architecture resembles a directed graph where each node n performs a process described by a transfer or else activation function f_n:

$$y_n = f_n\left(\sum_{i=1}^{m} \omega_{ni} x_i + b_n\right) \tag{4}$$

where y_n is the output of the node n, x_i is the ith input to the node, ω_{ni} is the connection weight between the n and i nodes and b_n is the threshold or else bias of the node. The activation function is usually nonlinear, such as the sigmoid, Heaviside or Gaussian functions. Through this process, a set of inputs is transformed to a set of desired outputs. To obtain the desired output, the weights are adjusted through the learning via examples [37,38].

In addressing regression problems with time series data, recurrent neural networks (RNNs) are becoming increasingly popular. RNNs have been used for various applications with time series data [39,40]. Their operation is based on the use of the input data combined with previous outputs for making a prediction. RNN models that present a high level performance include long short-term memory (LSTM) and gated recurrent unit (GRU) [41,42].

Elman networks and Jordan networks are popular simple RNNs (SRNs) that are used in this study. Elman [43] as well as Jordan [44] networks consist of three layers. Below, the mathematical formulations for the hidden and layer vector and output vector are given for both networks.

Elman network

$$h_t = \sigma_h(W_h x_t + U_h h_{t-1} + b_h) \tag{5}$$

$$y_t = \sigma_y(W_y h_t + b_y) \tag{6}$$

Jordan network

$$h_t = \sigma_h(W_h x_t + U_h y_{t-1} + b_h) \tag{7}$$

$$y_t = \sigma_y(W_y h_t + b_y) \tag{8}$$

where x_t is the input vector, h_t is the hidden layer vector, y_t is the output vector, σ_h and σ_y are the activation functions and W_h, W_y, U_h, U_y, b_h and b_y are the parameter matrices and vectors.

The multilayer perceptron (MLP) is the most common neural network. It generates a nonlinear model for prediction based on supervised training procedures. The MLP is a layered feedforward neural network where the information is transferred from the input layer unidirectionally to the output layer via the hidden layers [45]. Time-lag recurrent networks (TLRNs) are MLPs with short-term memory structures and local recurrent connections. The input layer uses the inputs delayed by multiple time points before being presented to the network [46]. The memory structures are characterized by the Laguerre memory and delay operator:

$$L_i(z,u) = \sqrt{1-(1-u)^2}\,\frac{\left(z^{-1}-(1-u)\right)^{i-1}}{\left(1-(1-u)z^{-1}\right)^{i}} \tag{9}$$

where L_i is the ith Laguerre function in the z-domain, u is a free parameter that represents the memory resolution and z^{-1} is the delay operator [47].

A generalized regression neural network (GRNN) consists of an improvement of the radial basis neural network (Figure 1). The advantages of the GRNN include strong nonlinear mapping ability and learning speed. The GRNN can have a very good prediction effect with small or unstable data [48–50]. The prediction value $Y(x)$ of input x is given from:

$$Y(x) = \frac{\sum_{i=1}^{N} w_i K(x, x_i)}{\sum_{i=1}^{N} K(x, x_i)} \tag{10}$$

where w_i is the activation function for the pattern layer neuron at i and $K(x, x_i)$ is a radial basis function kernel, such as the Gaussian kernel:

$$K(x, x_i) = e^{-d_k/2\sigma^2} \tag{11}$$

where $d_k = (x - x_i)^T(x - x_i)$ is the squared Euclidean distance between the training samples x_i and the input x.

A self-organizing feature map (SOFM) is a type of ANN that uses unsupervised learning in the training process to produce a map with reduced dimensionality compared to the input. The map is a low-dimensional, discretized representation of the input space of the training samples. The SOFM applies competitive learning by using a neighborhood function to preserve the topological properties of the input space [51].

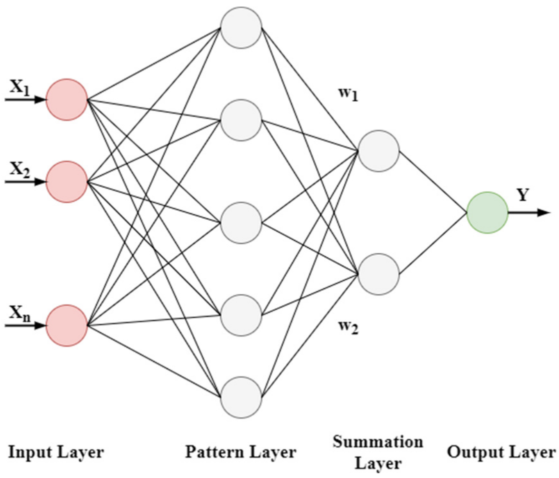

Figure 1. General structure of GRNN based on description contained in [52,53].

The generalized feedforward neural network (GFNN) architecture follows one of the feedforward neural networks (Figure 2). The Feedforward neural networks consist of at least 3 layers, namely the input layer, the hidden layer and the output layer. GFNN uses a generalized shunting neuron (GSN) model as the basic computing unit [50,54]. In the GFNN, the activity of the neurons can be described by the nonlinear expression:

$$\frac{dx_i}{dt} = I_i - a_i x_i - f\left(\sum_j w_{ij} x_j\right) x_i + b_i \tag{12}$$

where x_i is the activity of the ith neuron, I_i is the input to the ith neuron, a_i is a positive constant that represents the passive decay rate of the neuron, w_{ij} is the weight from the jth input to the ith neuron, b_i is the bias and f is the activation function.

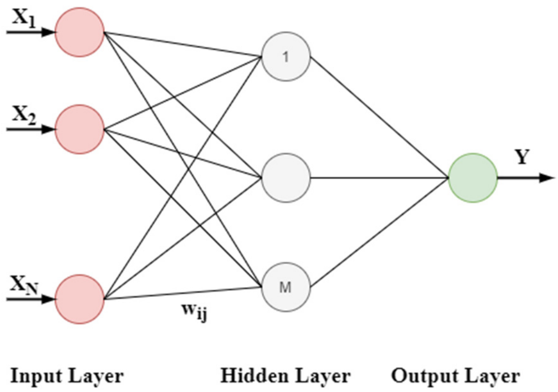

Figure 2. General structure of GFNN based on description contained in [52,53].

2.2.3. Post Hoc Explainability

To interpret the results and the contribution of the most important variable to the prediction output, a post hoc explainability analysis was performed by using Shapley additive explanations (SHAP). SHAP calculates optimal Shapley values from coalitional game theory. These values show how fairly the impact on a model's prediction is distributed among the variables of the dataset. Then, a mini-explainer model is developed that corresponds to a single-row-prediction pair in order to explain how this prediction was achieved [55–59].

3. Results

3.1. Evaluation Methodology

The proposed methodology was applied to the case study for the forecast of the LNG carrier charter rates, and it was implemented using the time series data presented in Section 2. Time series data from 1 January 2010 to 1 January 2017 were used. The aim was to predict the desired prediction variable, LNG 145K CBM spot rate, for the following dates: (i) 1 March 2017, (ii) 1 May 2017 and 1 July 2017. The methodology is composed of four main steps: (i) data collection; (ii) variable selection; (iii) comparative evaluation of popular time series forecast models; (iv) post hoc explainability analysis of the best performing model (Figure 3).

Figure 3. The four main steps of the methodology.

The study was implemented in Python on a Microsoft Windows 10 Environment operating system with an AMD Ryzen 7 3800X 8-Core Processor at 3.89 GHz and 32GB RAM. In Table 2, these values are presented.

Table 2. Real values for the time series LNG 145K CBM spot rate for the prediction dates.

LNG 145K CBM Spot Rate	Value (USD/Day)
1 March 2017	31,681
1 May 2017	34,768
1 July 2017	37,854

Initially, correlation analysis was performed to identify the variables that contribute to the development of the prediction models. To this end, PCC analysis was applied. In general, correlation is used to find the relationship between two variables to predict the value of one variable with the help of other correlated variables. A positive correlation result means both metrics increase in relation to each other, while a negative correlation means that as one metric increases, the other decreases. Table 3 shows the values of the PCC and their interpretation with respect to the correlation of the variables in this study.

Table 3. PCC values and correlation.

Value	Correlation
1	total positive linear correlation
-1	total negative linear correlation
$> \|0.2\|$	no linear correlation
$\|0.2–0.3\|$	low–medium linear correlation
$\|0.3–0.5\|$	medium linear correlation
$\|0.5–0.6\|$	medium–high linear correlation
$< \|0.6\|$	high linear correlation

The variables rounded to zero were considered as variables with no or low linear correlation with the decision variable, and thus they were excluded from our analysis.

Following the variable selection, the training of the prediction models was performed. To evaluate the performance of the models, the mean squared error (MSE) was used:

$$MSE = \frac{\sum_{j=0}^{P} \sum_{i=0}^{N} \left(d_{ij} - y_{ij}\right)^2}{N \cdot P} \tag{13}$$

where P is the number of output process elements, N is the number of iterations, y_{ij} is the output of ith iteration in the process element j and d_{ij} is the desired output for the ith iteration in process element j.

In Table 4 the ANN models used in this study and their parameter settings are presented.

Table 4. Summary of the parameters and the data used in the study.

Neural Networks	
Name	**Number of Parameters**
Multilayer Perceptron (MLP)	4 (Hidden Layers)
Generalized Feedforward (GFFN)	4 (Hidden Layers)
Modular Neural Network (MNN)	4 (Types)
Jordan/Elman Network	4 (Types)
General Regression Neural Network (GRNN)	4 (Hidden Layers)
Self-Organizing Feature Map Network (SOFM)	4 (Hidden Layers)
Time-Lag Recurrent Network (TLRN)	4 (Hidden Layers)
Variables for Prediction	
Name	**Prediction Time**
LNG 145K CBM Spot Rate	2 months
LNG 145K CBM Spot Rate	4 months
LNG 145K CBM Spot Rate	6 months
Data allocation	
Name	**Percentage**
Training data	75%
Testing data	10%
Cross validation data	15%
Number of epochs	
1000	

3.2. Results

From the PCC analysis we obtained the following results, shown in Table 5. From the results, we observed that some variables show low to moderate correlation or even none at all. That is, they are unrelated to the predictor variable. Therefore, these variables were excluded from our study. Specifically, the variables World Seaborne LNG Trade, Price of Liquefied U.S. Natural Gas Exports, Henry Hub Natural Gas Spot Price and New Orders Placed were discarded due to no or low linear correlation with the prediction variable, LNG 145K CBM spot rate, as shown in Table 6.

Table 5. Correlation coefficients between the prediction variable and the other variables for 2, 4 and 6 months.

Name of Variable	LNG 145K CBM Spot Rate *2 Months*	LNG 145K CBM Spot Rate *4 Months*	LNG 145K CBM Spot Rate *6 Months*
LNG 145K CBM Spot Rate	0.987	0.964	0.933
LNG 160K CBM Spot Rate	0.964	0.929	0.889
World Seaborne LNG Trade (Million Tonnes)	−0.676	−0.690	−0.699
World Seaborne LNG Trade (Billion Tonne-Miles)	*−0.115*	*−0.172*	*−0.222*
LNG 160K CBM 1 Year Timecharter Rate	0.933	0.897	0.855
Price of Liquefied U.S. Natural Gas Exports	*0.217*	*0.206*	*0.193*
Henry Hub Natural Gas Spot Price	*0.221*	*0.248*	*0.272*
Import LNG Japan Price	0.789	0.742	0.700
WTI Oil Price	0.666	0.626	0.593
Brent Oil Price	0.729	0.683	0.639
Total LNG Fleet	−0.915	−0.929	−0.935
Total Shipping Capacity	−0.901	−0.915	−0.921
Operational Capacity	−0.909	−0.932	−0.945
New Orders Placed	*0.294*	*0.265*	*0.243*
Orderbook	−0.726	−0.776	−0.816
Ships Delivered That Year	−0.934	−0.925	−0.906
Liquefaction Plants/Liquefaction	−0.815	−0.827	−0.834
Liquefaction Plants/Storage	−0.885	−0.906	−0.917
Regasification Plants/Storage	−0.838	−0.871	−0.895
Regasification Plants/Sent Out	−0.839	−0.874	−0.901
Spot LNG Imports	−0.700	−0.746	−0.783
Worldwide Natural Gas Production	−0.821	−0.858	−0.886
Worldwide Natural Gas Consumption	−0.804	−0.837	−0.863

Table 6. Variables with no or low correlation with the prediction variable.

Name of Variable	LNG 145K CBM Spot Rate *2 Months*	LNG 145K CBM Spot Rate *4 Months*	LNG 145K CBM Spot Rate *6 Months*
World Seaborne LNG Trade (Billion Tonne-Miles)	no correlation	no correlation	low–medium correlation
Price of Liquefied U.S. Natural Gas Exports	low–medium correlation	low–medium correlation	no correlation
Henry Hub Natural Gas Spot Price	low–medium correlation	low–medium correlation	low–medium correlation
New Orders Placed	low–medium correlation	low–medium correlation	low–medium correlation

The results show that all the rate (spot and time-charter) variables have very high positive correlation with the desired output. High negative correlation was also observed between the desired decision variable and the variables that show the total shipping capacity (total LNG fleet, total shipping capacity, operational capacity, etc.). To this end, these variables were excluded from the training of the predictive models.

The remaining variables were used to train the prediction models for the forecast periods of 2, 4 and 6 months of the LNG 145K m^3 spot rate. Tables 7–9 show the results for the trained models.

Table 7. Results of forecast for LNG 145K CBM spot rate: 2 months. The best score is shown in bold.

Neural Model	Type	LNG 145K CBM Spot Rate: 2 Months	
		Mean Squared Error (MSE)	
		Training	*Cross Validation*
Multilayer Perceptron	1 Hidden Layer	2.04177×10^{-6}	1.26952×10^{-4}
Multilayer Perceptron	2 Hidden Layers	1.02071×10^{-6}	2.71574×10^{-4}
Multilayer Perceptron	3 Hidden Layers	8.30945×10^{-8}	2.49368×10^{-4}
Multilayer Perceptron	4 Hidden Layers	4.04827×10^{-6}	1.9093×10^{-4}
Generalized Feedforward	1 Hidden Layer	8.13606×10^{-5}	6.953×10^{-4}
Generalized Feedforward	2 Hidden Layers	8.51169×10^{-7}	4.92954×10^{-4}
Generalized Feedforward	3 Hidden Layers	1.22216×10^{-25}	1.14536×10^{-4}
Generalized Feedforward	4 Hidden Layers	4.80591×10^{-16}	$\mathbf{9.0676 \times 10^{-5}}$
Modular Neural Network	Type 1	1.57247×10^{-10}	1.37449×10^{-4}
Modular Neural Network	Type 2	1.34044×10^{-8}	2.68479×10^{-4}
Modular Neural Network	Type 3	7.46558×10^{-9}	2.95709×10^{-4}
Modular Neural Network	Type 4	1.12069×10^{-9}	3.00228×10^{-4}
Jordan/Elman Network	Type 1	7.34076×10^{-6}	2.84278×10^{-4}
Jordan/Elman Network	Type 2	0.000400029	2.2034×10^{-4}
Jordan/Elman Network	Type 3	6.49497×10^{-5}	2.67897×10^{-4}
Jordan/Elman Network	Type 4	4.18497×10^{-6}	1.91801×10^{-4}
Generalized Regression Neural Network	1 Hidden Layer	8.96735×10^{-7}	2.41314×10^{-4}
Generalized Regression Neural Network	2 Hidden Layers	1.21131×10^{-9}	1.50232×10^{-4}
Generalized Regression Neural Network	3 Hidden Layers	3.44779×10^{-9}	2.30269×10^{-4}
Generalized Regression Neural Network	4 Hidden Layers	1.76621×10^{-7}	9.18787×10^{-5}
Self-Organized Feature Map Network	1 Hidden Layer	5.71591×10^{-13}	1.645705×10^{-3}
Self-Organized Feature Map Network	2 Hidden Layers	4.08174×10^{-29}	3.566318×10^{-3}
Self-Organized Feature Map Network	3 Hidden Layers	4.60911×10^{-11}	2.05648×10^{-4}
Self-Organized Feature Map Network	4 Hidden Layers	1.16882×10^{-9}	$1.31393527 \times 10^{-1}$
Time-Lag Recurrent Network	1 Hidden Layers	2.074106×10^{-3}	1.63206×10^{-3}
Time-Lag Recurrent Network	2 Hidden Layers	1.7725692×10^{-2}	2.3123×10^{-4}
Time-Lag Recurrent Network	3 Hidden Layers	1.0047504×10^{-2}	5.37872×10^{-4}
Time-Lag Recurrent Network	4 Hidden Layers	1.4389702×10^{-2}	2.38308×10^{-4}

Table 8. Results of forecast for LNG 145K CBM spot rate: 4 months. The best score is shown in bold.

Neural Model	Type	LNG 145K CBM Spot Rate: 4 Months	
		Mean Squared Error (MSE)	
		Training	*Cross Validation*
Multilayer Perceptron	1 Hidden Layer	3.741×10^{-6}	3.72×10^{-4}
Multilayer Perceptron	2 Hidden Layers	1.42506×10^{-7}	4.28×10^{-4}
Multilayer Perceptron	3 Hidden Layers	4.28696×10^{-8}	$\mathbf{8.09547 \times 10^{-5}}$
Multilayer Perceptron	4 Hidden Layers	1.99132×10^{-8}	2.33×10^{-4}
Generalized Feedforward	1 Hidden Layer	6.39153×10^{-6}	1.02×10^{-4}
Generalized Feedforward	2 Hidden Layers	2.82904×10^{-11}	2.42×10^{-4}
Generalized Feedforward	3 Hidden Layers	2.39175×10^{-25}	1.20×10^{-4}
Generalized Feedforward	4 Hidden Layers	4.44123×10^{-26}	9.26663×10^{-5}

Table 8. *Cont.*

Neural Model	Type	LNG 145K CBM Spot Rate: 4 Months Mean Squared Error (MSE) *Training*	*Cross Validation*
Modular Neural Network	Type 1	8.50244×10^{-9}	3.71×10^{-4}
Modular Neural Network	Type 2	4.58×10^{-4}	1.76×10^{-3}
Modular Neural Network	Type 3	1.78094×10^{-18}	2.84×10^{-4}
Modular Neural Network	Type 4	9.76073×10^{-10}	1.28×10^{-4}
Jordan/Elman Network	Type 1	1.1566×10^{-5}	1.18×10^{-4}
Jordan/Elman Network	Type 2	2.96119×10^{-5}	1.52×10^{-4}
Jordan/Elman Network	Type 3	3.64×10^{-4}	5.33×10^{-4}
Jordan/Elman Network	Type 4	1.95111×10^{-5}	6.20×10^{-4}
Generalized Regression Neural Network	1 Hidden Layer	1.36243×10^{-6}	1.35×10^{-4}
Generalized Regression Neural Network	2 Hidden Layers	7.19216×10^{-10}	3.34×10^{-4}
Generalized Regression Neural Network	3 Hidden Layers	9.0162×10^{-8}	2.03×10^{-4}
Generalized Regression Neural Network	4 Hidden Layers	2.48142×10^{-8}	5.31×10^{-4}
Self-Organized Feature Map Network	1 Hidden Layer	9.06784×10^{-27}	1.68×10^{-1}
Self-Organized Feature Map Network	2 Hidden Layers	2.23852×10^{-6}	1.86×10^{-3}
Self-Organized Feature Map Network	3 Hidden Layers	8.6554×10^{-27}	5.98×10^{-2}
Self-Organized Feature Map Network	4 Hidden Layers	1.16815×10^{-27}	8.81×10^{-2}
Time-Lag Recurrent Network	1 Hidden Layer	2.16×10^{-2}	4.80×10^{-4}
Time-Lag Recurrent Network	2 Hidden Layers	6.80×10^{-3}	4.45×10^{-4}
Time-Lag Recurrent Network	3 Hidden Layers	1.72×10^{-2}	1.71×10^{-3}
Time-Lag Recurrent Network	4 Hidden Layers	1.98×10^{-2}	6.71×10^{-4}

Table 9. Results of forecast for LNG 145K CBM spot rate: 6 months. The best score is shown in bold.

Neural Model	Type	LNG 145K CBM Spot Rate: 6 Months Mean Squared Error (MSE) *Training*	*Cross Validation*
Multilayer Perceptron	1 Hidden Layer	2.3057×10^{-6}	2.74×10^{-4}
Multilayer Perceptron	2 Hidden Layers	3.57161×10^{-7}	4.2437×10^{-5}
Multilayer Perceptron	3 Hidden Layers	1.28371×10^{-6}	4.94×10^{-4}
Multilayer Perceptron	4 Hidden Layers	2.80881×10^{-6}	7.28×10^{-4}
Generalized Feedforward	1 Hidden Layer	4.12988×10^{-6}	3.40×10^{-4}
Generalized Feedforward	2 Hidden Layers	2.9611×10^{-26}	1.59×10^{-4}
Generalized Feedforward	3 Hidden Layers	1.47921×10^{-29}	4.85×10^{-3}
Generalized Feedforward	4 Hidden Layers	3.96904×10^{-27}	8.58066×10^{-5}
Modular Neural Network	Type 1	5.34594×10^{-8}	2.76×10^{-4}
Modular Neural Network	Type 2	2.00206×10^{-16}	2.56×10^{-3}
Modular Neural Network	Type 3	8.28519×10^{-10}	4.45×10^{-4}

Table 9. *Cont.*

Neural Model	Type	LNG 145K CBM Spot Rate: 6 Months	
		Mean Squared Error (MSE)	
		Training	*Cross Validation*
Modular Neural Network	Type 4	8.34674×10^{-7}	7.59×10^{-4}
Jordan/Elman Network	Type 1	1.02852×10^{-5}	5.57×10^{-4}
Jordan/Elman Network	Type 2	7.33229×10^{-5}	5.47×10^{-4}
Jordan/Elman Network	Type 3	3.06×10^{-4}	9.83×10^{-4}
Jordan/Elman Network	Type 4	5.30217×10^{-6}	6.06×10^{-4}
Generalized Regression Neural Network	1 Hidden Layer	3.00376×10^{-7}	7.78351×10^{-5}
Generalized Regression Neural Network	2 Hidden Layers	2.59021×10^{-8}	1.27×10^{-3}
Generalized Regression Neural Network	3 Hidden Layers	1.23496×10^{-19}	$\mathbf{3.51658 \times 10^{-5}}$
Generalized Regression Neural Network	4 Hidden Layers	5.70×10^{-2}	8.91×10^{-3}
Self-Organized Feature Map Network	1 Hidden Layer	3.77435×10^{-15}	3.70×10^{-3}
Self-Organized Feature Map Network	2 Hidden Layers	3.99304×10^{-27}	9.17×10^{-4}
Self-Organized Feature Map Network	3 Hidden Layers	1.50628×10^{-23}	7.75×10^{-2}
Self-Organized Feature Map Network	4 Hidden Layers	2.97364×10^{-15}	8.74×10^{-3}
Time-Lag Recurrent Network	1 Hidden Layer	3.71×10^{-2}	7.72×10^{-4}
Time-Lag Recurrent Network	2 Hidden Layers	1.20×10^{-2}	2.10×10^{-4}
Time-Lag Recurrent Network	3 Hidden Layers	1.50×10^{-2}	7.79×10^{-4}
Time-Lag Recurrent Network	4 Hidden Layers	2.85×10^{-2}	7.56×10^{-4}

Figures 4–6 illustrate the summary plots of SHAP analysis for the best performing models of the LNG 145K CBM spot rate forecast for 2, 4 and 6 months, respectively.

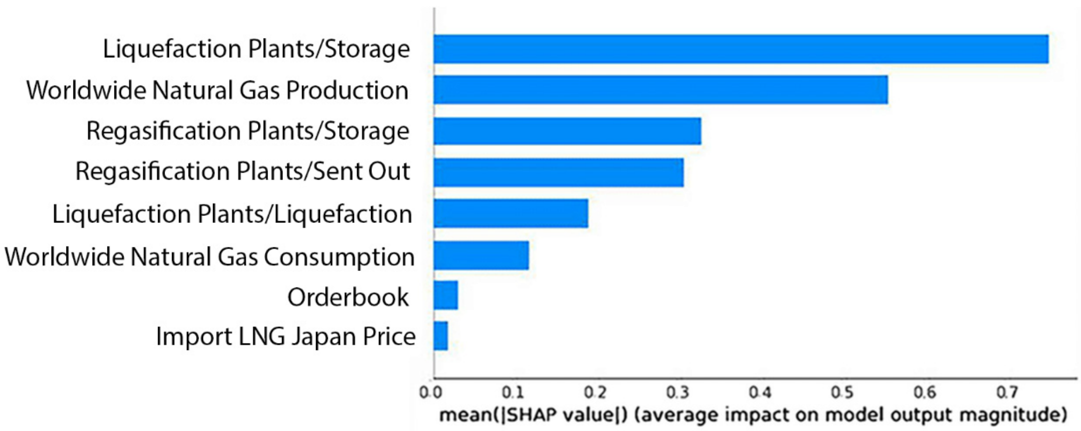

Figure 4. SHAP summary plot for LNG 145K CBM spot rate: 2 months of GFFN model.

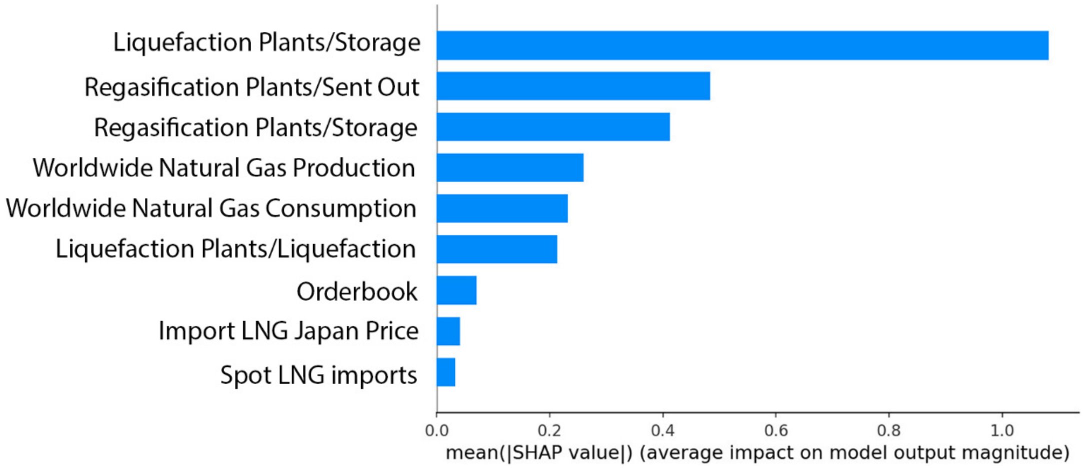

Figure 5. SHAP summary plot for LNG 145K CBM spot rate: 4 months of MLP model.

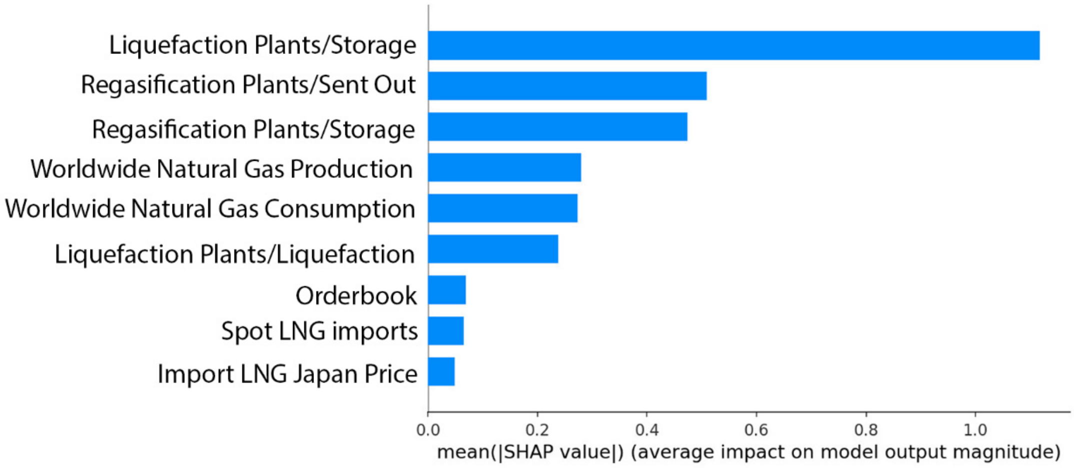

Figure 6. SHAP summary plot for LNG 145K CBM spot rate: 6 months of GRNN model.

4. Discussion

This study contributes to literature by conducting a thorough comparative evaluation of popular NNs to test their ability for short and mid-term predictions of the spot charter rate in the case of LNG carriers. Specifically, the following artificial neural network models were applied to forecast the LNG 145K CBM spot rate for 2 months (1 March 2017), 4 months (1 May 2017) and 6 months (1 July 2017):

- Multilayer perceptron (MLP)
- Generalized feedforward (GFFN)
- Modular (programming)
- Jordan/Elman
- General regression neural network (GRNN)
- Self-organizing map (SOM)
- Time-lag recurrent network (TLRN).

The results from Table 7 show that the GFFN architecture, with four hidden layers, results in a better forecast (MSE 9.0676×10^{-5}) for a very short forecast period (2 months); however, the GRNN with four hidden layers presented a competitive performance (MSE 9.18787×10^{-5}). Regarding the short-term prediction of 4 months shown in Table 8, the MLP with three hidden layers achieved the best performance (MSE 8.09547×10^{-5}). In the case of mid-term forecast (6 months), as shown in Table 9, GRNN networks reached the best performance with three hidden layers (MSE 3.51658×10^{-5}). However, MLP (MSE 4.2437×10^{-5}) and GFFN (MSE 8.58066×10^{-5}) networks presented a competitive performance.

Overall, we can say that the GRNN architecture presented a more stable performance with respect to the forecast period in all cases. Thus, a more accurate prediction model for the freight price of LNG carriers can be built by using GRNN networks.

For the post hoc explainability analysis, the SHAP model was employed. Figures 4–6 illustrate the summary plot with the eight variables with the highest contribution to the prediction output of the best performing model for the LNG 145K CBM spot rate for 2, 4 and 6 months, respectively. The analysis shows that almost the same variables proved to be most significant for the short and mid-term forecast of the prediction variable, a result that is in accordance with the initial variable selection and the correlation analysis.

5. Conclusions

In this study, a machine learning pipeline was presented to forecast the freight price of LNG carriers. The proposed methodology covers the gap in the literature regarding the LNG carrier freight market so as to facilitate the decision-making in the maritime industry. Specifically, the study focused on the prediction of the price of the daily fare for an LNG tanker with a capacity of 145,000 CBM and a steam turbine vessel. The methodology incorporates: (i) the collection of data relevant to LNG to form a dataset; (ii) the identification of the variables of the dataset that significantly contribute to the accurate prediction of the selected decision variable; (iii) the development of prediction machine learning models and (iv) the evaluation of model performance with respect to the mean squared error.

Overall, data from 1 January 2010 to 1 January 2017 were collected for 23 variables. The PCC showed that there was no linear correlation among the decision variable and the variables relevant to trades, contracts trades and new orders. Hence, from the 23 variables, only four were excluded from the analysis. The formed dataset was used to train various machine learning models, namely multilayer the MLP, GFFN, Jordan/Elman, GRNN, SOM and TLRN. The results showed that the GFFN with four hidden layers had the best performance for the 2-month forecast, the MLP with three hidden layers had the best performance for the 4-month forecast and the GRNN with four hidden layers had the best performance for 6-month forecast. However, the GRNN presented a stable and comparative performance in all cases. Therefore, a GRNN architecture can be considered as a suitable machine learning approach to develop a forecast model for the freight price of LNG carriers.

Future work includes further investigation of various types of machine learning models and extension of the work focusing on other types of LNG tankers, such as an LNG tanker with a capacity of 160,000 or 174,000 CBM. It can also include updated datasets and variables other than price (e.g., the marine environment, safety performance, risk analysis), where further development of the spot LNG shipping market will be reflected. Lastly, future studies can include long-term forecasting by taking into account the impact of the COVID-19 pandemic on the LNG market.

Funding: The author executed the study in the frame of research conducted for the BioSFerA project (https://biosfera-project.eu) funded by the European Union's Horizon 2020 research and innovation programme (Grant Agreement 884208).

Institutional Review Board Statement: Not applicable.

Informed Consent Statement: Not applicable.

Data Availability Statement: Not applicable.

Conflicts of Interest: The author declare no conflict of interest.

References

1. Awoyomi, A.; Patchigolla, K.; Anthony, E.J. Process and Economic Evaluation of an Onboard Capture System for LNG-Fueled CO2 Carriers. *Ind. Eng. Chem. Res.* **2020**, *59*, 6951–6960. [CrossRef]
2. Chu Van, T.; Ramirez, J.; Rainey, T.; Ristovski, Z.; Brown, R.J. Global Impacts of Recent IMO Regulations on Marine Fuel Oil Refining Processes and Ship Emissions. *Transp. Res. Part D Transp. Environ.* **2019**, *70*, 123–134. [CrossRef]
3. Seithe, G.J.; Bonou, A.; Giannopoulos, D.; Georgopoulou, C.A.; Founti, M. Maritime Transport in a Life Cycle Perspective: How Fuels, Vessel Types, and Operational Profiles Influence Energy Demand and Greenhouse Gas Emissions. *Energies* **2020**, *13*, 2739. [CrossRef]
4. Pavlenko, N.; Comer, B.; Zhou, Y.; Clark, N.; Rutherford, D. *The Climate Implications of Using LNG as a Marine Fuel*; Swedish Environmental Protection Agency: Stockholm, Sweden, 2020.
5. International Gas Union. *World Lng Report*; International Gas Union: Barcelona, Spain, 2020.
6. GIIGNL—International Group of Liquefied Natural Gas Importers. *GIIGNL Annual Report—The LNG Industry*; GIIGNL: Elmwood Park, NJ, USA, 2020.
7. International Energy Agency. *Global Gas Security Review 2019*; International Energy Agency: Paris, France, 2019.
8. Atsalakis, G.S. Using Computational Intelligence to Forecast Carbon Prices. *Appl. Soft Comput. J.* **2016**, *43*, 107–116. [CrossRef]
9. Dario, U. *Forecasting Energy Market: An Artificial Neural Network Approach*; Universita Ca'Foscari Venezia: Venice, Italy, 2015.
10. Wu, Y.H.; Hua, J.; Chen, H.L. Economic Feasibility of an Alternative Fuel for Sustainable Short Sea Shipping: Case of Cross-Taiwan Strait Transport. In Proceedings of the World Congress on New Technologies, Madrid, Spain, 19–21 August 2018.
11. Le Fevre, C.N. *A Review of Demand Prospects for LNG as a Marine Fuel*; Oxford Institute for Energy Studies: Oxford, UK, 2018.
12. Merien-Paul, R.H.; Enshaei, H.; Jayasinghe, S.G. Guessing to Prediction-a Conceptual Framework to Predict LNG Bunker Demand Profile in Australia. In Proceedings of the IAMU AGA 17-Working Together: The Key Way to Enhance the Quality of Maritime Education, Training and Research, Hải Phòng, Vietnam, 26–29 October 2016; pp. 244–252.
13. Aronietis, R.; Sys, C.; Van Hassel, E.; Vanelslander, T. Forecasting Port-Level Demand for LNG as a Ship Fuel: The Case of the Port of Antwerp. *J. Shipp. Trade* **2016**, *1*, 2. [CrossRef]
14. Arnet, N.M.L. LNG Bunkering Operations: Establish Probabilistic Safety Distances for LNG Bunkering Operations. Master's Thesis, Institutt for energi-Og Prosessteknikk, Trondheim, Norway, 2014.
15. Jin, J.; Kim, J. Forecasting Natural Gas Prices Using Wavelets, Time Series, and Artificial Neural Networks. *PLoS ONE* **2015**, *10*, e0142064. [CrossRef]
16. Al-Fattah, S.M.; Startzman, R.A. Predicting Natural Gas Production Using Artificial Neural Network. In Proceedings of the SPE Hydrocarbon Economics and Evaluation Symposium, Dallas, TX, USA, 2–3 April 2001.
17. Su, M.; Zhang, Z.; Zhu, Y.; Zha, D. Data-Driven Natural Gas Spot Price Forecasting with Least Squares Regression Boosting Algorithm. *Energies* **2019**, *12*, 1094. [CrossRef]
18. Busse, S.; Helmholz, P.; Weinmann, M. Forecasting Day Ahead Spot Price Movements of Natural Gas—An Analysis of Potential Influence Factors on Basis of a NARX Neural Network. In Proceedings of the Multikonferenz Wirtschaftsinformatik 2012—Tagungsband der MKWI 2012, Braunschweig, Germany, 21–22 March 2012.
19. Hosseinipoor, S. Forecasting Natural Gas Prices in the United States Using Artificial Neural Networks. Master's Thesis, University of Oklahoma, Norman, OK, USA, 2016.
20. Akpinar, M.; Adak, M.F.; Yumusak, N. Day-Ahead Natural Gas Demand Forecasting Using Optimized ABC-Based Neural Network with Sliding Window Technique: The Case Study of Regional Basis in Turkey. *Energies* **2017**, *10*, 781. [CrossRef]
21. Moraes, L.A.M.; Faria, L.F.T. A Stochastic Programming Approach to Liquified Natural Gas Planning. *Pesqui. Oper.* **2016**, *36*, 151–165. [CrossRef]
22. Engelen, S.; Norouzzadeh, P.; Dullaert, W.; Rahmani, B. Multifractal Features of Spot Rates in the Liquid Petroleum Gas Shipping Market. *Energy Econ.* **2011**, *33*, 88–98. [CrossRef]
23. Giannakopoulou, P.; Chountas, P. Forecasting the Spot Price of P1A Shipping Route. In Proceedings of the 2019 Big Data, Knowledge and Control Systems Engineering, BdKCSE 2019, Sofia, Bulgaria, 21–22 November 2019.
24. von Spreckelsen, C.; von Mettenheim, H.J.; Breitner, M.H. Short-Term Trading Performance of Spot Freight Rates and Derivatives in the Tanker Shipping Market: Do Neural Networks Provide Suitable Results? In *Communications in Computer and Information Science*; Springer: Berlin/Heidelberg, Germany, 2012.
25. von Spreckelsen, C.; von Mettenheim, H.-J.; Breitner, M.H. Spot and Freight Rate Futures in the Tanker Shipping Market: Short-Term Forecasting with Linear and Non-Linear Methods. In *Operations Research Proceedings*; Springer: Berlin/Heidelberg, Germany, 2014.
26. Lyridis, D.V.; Manos, N.D.; Zacharioudakis, P.G. Modeling the Dry Bulk Shipping Market Using Macroeconomic Factors in Addition to Shipping Market Parameters via Artificial Neural Networks. *Int. J. Transp. Econ.* **2014**, *41*, 231–253.
27. Yin, J.; Luo, M.; Fan, L. Dynamics and Interactions between Spot and Forward Freights in the Dry Bulk Shipping Market. *Marit. Policy Manag.* **2017**, *44*, 271–288. [CrossRef]
28. Yip, T.L. Predicting the Shipping Market by Spreads of Timecharter Rates. *Zesz. Nauk. Akad. Mor. W Szczec.* **2018**, *53*, 9–16.
29. Du, Q. Forecasting and Backtesting of VaR in International Dry Bulk Shipping Market under Skewed Distributions. *Am. J. Ind. Bus. Manag.* **2019**, *9*, 1168–1186. [CrossRef]

30. Cao, J.; Li, Z.; Li, J. Financial Time Series Forecasting Model Based on CEEMDAN and LSTM. *Phys. A: Stat. Mech. Appl.* **2019**, *519*, 127–139. [CrossRef]
31. Sagheer, A.; Kotb, M. Time Series Forecasting of Petroleum Production Using Deep LSTM Recurrent Networks. *Neurocomputing* **2019**, *323*, 203–213. [CrossRef]
32. Schober, P.; Schwarte, L.A. Correlation Coefficients: Appropriate Use and Interpretation. *Anesth. Analg.* **2018**, *126*, 1763–1768. [CrossRef]
33. Chen, P.Y.; Popovich, P.M. Correlation: Parametric and Nonparametric Measures. In *Correlation*; SAGE Publications, Inc.: Thousand Oaks, CA, USA, 2011.
34. Herbrich, R.; Graepel, T.; Obermayer, K. *Regression Models for Ordinal Data: A Machine Learning Approach*; Fachbereich 13, Informatik. TR-99/03; Technische Universität Berlin: Berlin, Germany, 1999.
35. Madsen, H. *Time Series Analysis*; Taylor & Francis eBooks: New York, NY, USA, 2007; ISBN 9781420059687.
36. Wang, K.; Li, K.; Zhou, L.; Hu, Y.; Cheng, Z.; Liu, J.; Chen, C. Multiple Convolutional Neural Networks for Multivariate Time Series Prediction. *Neurocomputing* **2019**, *360*, 107–119. [CrossRef]
37. Hassoun, M.H. Fundamentals of Artificial Neural Networks. *Proc. IEEE* **2005**, *84*, 906. [CrossRef]
38. Buscema, P.M.; Massini, G.; Breda, M.; Lodwick, W.A.; Newman, F.; Asadi-Zeydabadi, M. Artificial Neural Networks. In *Studies in Systems, Decision and Control*; Springer: Berlin/Heidelberg, Germany, 2018.
39. Laptev, N.; Yosinski, J.; Li, E.L.; Smyl, S. Time-Series Extreme Event Forecasting with Neural Networks at Uber. *Comput. Sci.* **2017**, *34*, 1–5.
40. Che, Z.; Purushotham, S.; Cho, K.; Sontag, D.; Liu, Y. Recurrent Neural Networks for Multivariate Time Series with Missing Values. *Sci. Rep.* **2018**, *8*, 6085. [CrossRef] [PubMed]
41. Caterini, A.L.; Chang, D.E. Recurrent Neural Networks. In *SpringerBriefs in Computer Science*; Springer: Berlin/Heidelberg, Germany, 2018.
42. Hewamalage, H.; Bergmeir, C.; Bandara, K. Recurrent Neural Networks for Time Series Forecasting: Current Status and Future Directions. *Int. J. Forecast.* **2020**, *37*, 388–427. [CrossRef]
43. Elman, J.L. Finding Structure in Time. *Cogn. Sci.* **1990**, *14*, 179–211. [CrossRef]
44. Jordan, M.I. Chapter 25 Serial Order: A Parallel Distributed Processing Approach. In *Advances in Psychology*; Elsevier: Amsterdam, The Netherlands, 1997.
45. Taud, H.; Mas, J.F. Multilayer Perceptron (MLP). In *Geomatic Approaches for Modeling Land Change Scenarios*; Springer: Cham, Switzerland, 2018; pp. 451–455.
46. Zhou, Y.; Xia, J.; Shen, H.; Zhou, J.; Wang, Z. Extended Dissipative Learning of Time-Delay Recurrent Neural Networks. *J. Frankl. Inst.* **2019**, *356*, 8745–8769. [CrossRef]
47. Dayhoff, J.; Omidvar, O. Locally Recurrent Networks: The Gamma Operator, Properties, and Extensions. In *Neural Networks and Pattern Recognition*; Oxford University Press: Cary, NC, USA, 1998.
48. Cigizoglu, H.K. Generalized Regression Neural Network in Monthly Flow Forecasting. *Civ. Eng. Environ. Syst.* **2005**, *22*, 71–81. [CrossRef]
49. Specht, D.F. A General Regression Neural Network. *IEEE Trans. Neural Netw.* **1991**, *2*, 568–576. [CrossRef]
50. Firat, M.; Gungor, M. Generalized Regression Neural Networks and Feed Forward Neural Networks for Prediction of Scour Depth around Bridge Piers. *Adv. Eng. Softw.* **2009**, *40*, 731–737. [CrossRef]
51. Nikoo, M.; Sadowski, Ł.; Khademi, F.; Nikoo, M. Determination of Damage in Reinforced Concrete Frames with Shear Walls Using Self-Organizing Feature Map. *Appl. Comput. Intell. Soft Comput.* **2017**, *2017*, 1–10. [CrossRef]
52. Ntakolia, C.; Anagnostis, A.; Moustakidis, S.; Karcanias, N. Machine Learning Applied on the District Heating and Cooling Sector: A Review. *Energy Syst.* **2022**, *13*, 1–30. [CrossRef]
53. Liu, H.; Yan, G.; Duan, Z.; Chen, C. Intelligent Modeling Strategies for Forecasting Air Quality Time Series: A Review. *Appl. Soft Comput.* **2021**, *102*, 106957. [CrossRef]
54. Arulampalam, G.; Bouzerdoum, A. A Generalized Feedforward Neural Network Architecture for Classification and Regression. *Neural Netw.* **2003**, *16*, 561–568. [CrossRef]
55. Ntakolia, C.; Kokkotis, C.; Moustakidis, S.; Tsaopoulos, D. Prediction of Joint Space Narrowing Progression in Knee Osteoarthritis Patients. *Diagnostics* **2021**, *11*, 285. [CrossRef] [PubMed]
56. Lundberg, S.M.; Lee, S.-I. A Unified Approach to Interpreting Model Predictions. In Proceedings of the 31st International Conference on Neural Information Processing Systems, Long Beach, CA, USA, 4–9 December 2017; Volume 30.
57. Ntakolia, C.; Kokkotis, C.; Karlsson, P.; Moustakidis, S. An Explainable Machine Learning Model for Material Backorder Prediction in Inventory Management. *Sensors* **2021**, *21*, 7926. [CrossRef] [PubMed]
58. Kokkotis, C.; Ntakolia, C.; Moustakidis, S.; Giakas, G.; Tsaopoulos, D. Explainable Machine Learning for Knee Osteoarthritis Diagnosis Based on a Novel Fuzzy Feature Selection Methodology. *Phys. Eng. Sci. Med.* **2022**, *45*, 219–229. [CrossRef]
59. Ntakolia, C.; Priftis, D.; Charakopoulou-Travlou, M.; Rannou, I.; Magklara, K.; Giannopoulou, I.; Kotsis, K.; Serdari, A.; Tsalamanios, E.; Grigoriadou, A.; et al. An Explainable Machine Learning Approach for COVID-19′s Impact on Mood States of Children and Adolescents during the First Lockdown in Greece. *Healthcare* **2022**, *10*, 149. [CrossRef] [PubMed]